Structure Investigation on Anhydrous Disodium Hydrogen Phosphate Using Solid-State NMR and X-ray Techniques

M. Baldus,[†,⊥] B. H. Meier,[†,⊥] R. R. Ernst,[†] A. P. M. Kentgens,[‡] H. Meyer zu Altenschildesche,[§] and R. Nesper*[,§]

Contribution from the Laboratorium für Physikalische Chemie, ETH Zentrum, CH-8092 Zürich, Switzerland, NSR Center for Molecular Structure, Design and Synthesis, Toernooiveld, NL-6525 ED Nijmegen, The Netherlands, and Laboratorium für Anorganische Chemie, ETH Zentrum, CH-8092 Zürich, Switzerland

Received November 30, 1994[⊗]

Abstract: Solid-state NMR and powder X-ray diffraction techniques are combined for the resolution of structural problems in the solid state. The crystal structure of anhydrous Na_2HPO_4 is reexamined. Sodium-23 NMR spectra under magic angle spinning and double rotation are interpreted in terms of chemical shift and quadrupole interaction parameters. An extended Floquet theory formalism is used to calculate the spectra. The three inequivalent sodium sites found are consistent with a $P2_1/c$ crystal structure rather than with the previously published $P2_1/m$ structure. Powder X-ray data are in accordance with the NMR results and are used to obtain improved atomic coordinates.

Introduction

In X-ray crystallography studies, it is sometimes difficult to uniquely determine the molecular structure and the associated space group, in particular when the possible structures differ mainly in hydrogen positions. Additional structure-sensitive measurements are then desired. It is known that neutron-diffraction data are especially sensitive to the deuterium sites in the corresponding deuterated compounds and are useful as complements. On the other hand, solid-state nuclear magnetic resonance (NMR) measurements prove to be quite informative about local structural distortions that lead to inequivalent sites and lower space group symmetry. This is demonstrated in this paper by an investigation of the crystal structure of anhydrous disodium hydrogen phosphate.

Anhydrous disodium hydrogen phosphate (Na_2HPO_4) has been reported to crystallize in a monoclinic structure of space group $P2_1/m$ (in the following called model A).[1] Due to the difficulties in obtaining single crystals of high quality, the final residual value of this study remained at a relatively high value of $R = 0.09$. The authors suggested a disordered room temperature structure and found no indications of a superstructure required for an ordered arrangement. The postulated disorder involves predominantly the protons that are distributed between two equally populated sites.

Earlier heat capacity measurements in the range 10−320 K gave no indication for phase transitions nor did they show any residual entropy due to disorder at low temperatures.[2] The possibility of space groups with lower symmetry, such as $P2_1/a$, $P2_1/c$, or $P2_1/n$, was recently mentioned.[3] These space groups lead to a doubling of the unit cell associated with the loss of the mirror plane and would allow for ordered structures that are consistent with the experimental data.

Nuclear magnetic resonance (NMR) can provide information that may allow the selection of the proper symmetry group. The local symmetry at the sodium sites is reflected by the electrical quadrupolar interaction and the chemical shift interaction. Both interactions allow one to distinguish between sodium sites with different electronic environments and are sensitive probes for the space group. To resolve the inequivalent sites, magic angle spinning (MAS) is necessary. For sodium with a spin $^3/_2$ and three allowed transitions, the central transition ($m_I = {}^1/_2 \rightarrow -{}^1/_2$) is particularly narrow because it is only affected by the quadrupolar interaction in second order. Under sample spinning at typical frequencies of 5−15 kHz, this transition shows up as an intense signal whereas the other two transitions, which are influenced by the quadrupolar interaction already in first order, are split into a larger number of low-intensity rotational sidebands.

A further line narrowing of the central transition is obtained by simultaneous double rotation (DOR) or sequential dynamic angle spinning (DAS) two-axis rotation techniques[4−9] that average out, in the fast rotation limit, the second-order quadrupolar interaction. The resulting DOR and DAS $m_I = \pm{}^1/_2$ spectra consist of sharp resonance lines and allow one to spectrally distinguish chemically inequivalent sites. The chemical shift and quadrupolar coupling anisotropy can be extracted from the sideband amplitudes by means of numerical simulation and fitting techniques.[10,11]

[†] Laboratorium für Physikalische Chemie, ETH Zentrum.
[‡] NSR Center for Molecular Structure, Design and Synthesis.
[§] Laboratorium für Anorganische Chemie, ETH Zentrum.
[⊥] Current address: Laboratory of Physical Chemistry, University of Nijmegen, Toernooiveld, NL-6525 ED Nijmegen, The Netherlands.
[⊗] Abstract published in *Advance ACS Abstracts,* April 15, 1995.

(1) Wiench, D. M.; Jansen, M. Z. *Z. Anorg. Allg. Chem.* **1983**, *501*, 95−101.
(2) Andon, R. J. L.; Counsell, J. F.; Martin, J. F.; Mash, C. J. *J. Appl. Chem.* **1967**, *17*, 65−70.
(3) Templeton, D. H.; Ruben, H. W.; Zalkin, A. *J. Phys. Chem.* **1990**, *94*, 7830−7834.
(4) Llor, A.; Virlet, J. *Chem. Phys. Lett.* **1988**, *152*, 248−253.
(5) Samoson, A.; Lippmaa, E.; Pines, A. *Mol. Phys.* **1988**, *65*, 1013−1018.
(6) Chmelka, B. F.; Mueller, K. T.; Pines, A.; Stebbins, J.; Wu, Y.; Zwanziger, J. W. *Nature (London)* **1989**, *339*, 42−43.
(7) Mueller, K. T.; Sun, B. Q.; Chingas, G. C.; Zwanziger, J. W.; Terao, T.; Pines, A. *J. Magn. Reson.* **1990**, *86*, 470−487.
(8) Wu, Y.; Sun, B. Q.; Pines, A.; Samoson, A.; Lippmaa, E. *J. Magn. Reson.* **1990**, *89*, 297−309.
(9) Chmelka, B. F.; Zwanziger, J. W. In *NMR Basic Principles Progress*; Kosfeld, P., Blümich, B., Eds.; Springer: Berlin, 1994; Vol. 33, pp 79−124.
(10) Sun, B. Q.; Baltisberger, J. H.; Wu, Y.; Samoson, A.; Pines, A. *Solid State NMR* **1992**, *1*, 267−295.
(11) (a) Cochon, E.; Amoureux, J. P. *Solid State NMR* **1993**, *2*, 205−222. (b) Amoureux, J. P.; Cochon, E. *Solid State NMR* **1993**, *2*, 223−234.

0002-7863/95/1517-5141$09.00/0

For spectra with considerable overlap, an elegant extension of the two-dimensional DAS experiment has recently been proposed[9,12,13] which allows one to correlate the isotropic spin interaction of each site with its second-order quadrupolar pattern. This experiment requires in each scan two rapid reorientations of the spinner axis.

For anhydrous Na_2HPO_4, one-dimensional MAS and DOR spectra are sufficient to obtain the desired structural information. These spectra can be recorded in the absence of rf pulses, and no delays are required for changes of axis direction. Therefore, these spectra are particularly well suited for quantitative evaluations. Such an analysis shows that the previously reported space group is incorrect. With the knowledge of the correct number and multiplicity of distinguishable sodium sites, an improved structure refinement within the proper space group is possible. The combination of NMR and powder X-ray diffraction (XRD) measurements gives convincing evidence that anhydrous Na_2HPO_4 crystallizes in space group $P2_1/c$ (in the following called model B).

Experiments and Calculations

Anhydrous Na_2HPO_4 was obtained in 99.5% purity from Fluka Chemie (Switzerland). The analysis of powder XRD data confirmed a homogeneous crystalline phase. ^{23}Na nonsynchronized DOR and MAS NMR experiments were performed at 11.7 T magnetic field strength using a Bruker ASX500 spectrometer and at 7 T using a home-built spectrometer with a 5 mm Doty MAS probehead. For all experiments, 100−500 acquisitions were averaged using excitation pulses of 1−2 μs and recycle delays of 1 s. The MAS spectra were recorded under proton decoupling with a field strength of 50 kHz. Chemical shift values are reported relative to an aqueous 0.1 M solution of NaCl.

All numerical simulations of the rotating and double-rotating experiments were performed with the program library GAMMA[14,15] using an extended Floquet formalism.[16] Powder spectra were calculated by a simultaneous incrementation method of the Euler angles.[17] The overall computation time on an IBM RS/6000 workstation was less than 1 h for MAS experiments and 4−10 h for nonsynchronized DOR spectra. For the numerical fitting procedures described below, the Fortran routine MINUIT was used.[18]

Powder XRD measurements were performed on a STOE Stadi-P diffractometer equipped with a position-sensitive detector (resolution 0.01° in 2θ) and a curved Ge monochromator. The sample was finely ground and filled into a 0.3 mm outer diameter glass capillary. Monochromatic Cu $K\alpha_1$ radiation of wavelength 0.154056 nm was used to measure the diffraction intensity data over the range $7.00 \leq 2\theta \leq 87.98°$ with a step size of 0.02°. The total measuring time was 31 h. Finally, the structure was determined using the Rietveld refinement method from the program package XRS-82.[19]

Results and Discussion

(a) NMR Experiments and Simulations. The sampling points of the ^{23}Na MAS spectrum, recorded at 11.7 T and a spinning speed of 14 kHz, are shown in Figure 1. The spectrum shows the superposition of several second-order quadrupolar centerband patterns ($m_I = 1/2 \rightarrow -1/2$). The five visually distinct peaks suggest that at least three sites must contribute to the overall line shape.

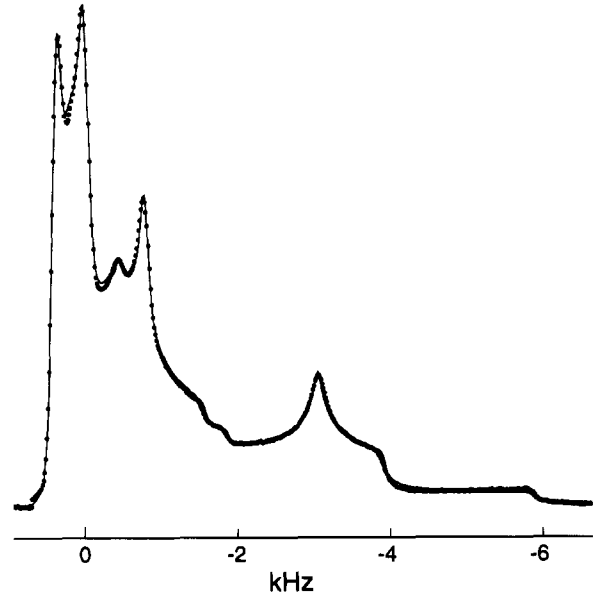

Figure 1. Sampling points of the ^{23}Na MAS spectrum of anhydrous Na_2HPO_4 at 14 kHz spinning frequency and 11.7 T magnetic field strength. Chemical shift values are given with reference to an aqueous 0.1 M solution of NaCl. The solid line represents the least-squares-fitted spectrum using the parameters of Table 1.

In order to obtain more information about the number of sodium sites, DOR experiments were carried out. DOR spectra for two different sets of spinning speeds are presented in Figure 2. A comparison reveals that the positions of the three strongest peaks are independent of the spinning speed. Consequently, these resonances represent the central bands of three sideband patterns.

Numerical simulations were performed to investigate whether both types of experiments can be described by the same set of quadrupolar parameters. We consider a quadrupolar spin system in the presence of a strong external magnetic field with the Hamiltonian

$$H = H_Z + H_Q + H_{CSA} + H_{DD} \quad (1)$$

The anisotropic chemical shift (CSA) and the dipolar interaction (DD) are assumed to be much weaker than the quadrupolar contribution:

$$||H_Z|| \gg ||H_Q|| \gg ||H_{CSA}||, ||H_{DD}|| \quad (2)$$

It is then justified to treat the quadrupolar part H_Q of the total Hamiltonian (and the chemical shift and dipolar contributions) as a small perturbation to the dominating Zeeman interaction H_Z and to neglect cross terms between H_Q, H_{CSA}, and H_{DD}. The Hamiltonian for the central transition (ct) is then of the form:

$$H^{(ct)}(t) = H_Q^{(2)} + H_{CSA} + H_{DD} \quad (3)$$

with the second-order quadrupolar interaction

$$H_Q^{(2)} = \sum_i \frac{\omega_{Q,i}^2}{2\omega_0} \sum_{m=-2}^{2} \frac{1}{m} G_m^{Lab,(i)}(t)[T_{2m}^{(i)}, T_{2,-m}^{(i)}] \quad (m \neq 0) \quad (4)$$

where the index i runs over all quadrupolar spins.

For fast sample rotation, the three contributions to the Hamiltonian of eq 3 can be averaged separately over a rotation period; the dipolar contribution vanishes and the anisotropic chemical

(12) Baltisberger, S. H.; Gann, S. L.; Wooten, E. W.; Chang, T. H.; Mueller, K. T.; Pines, A. *J. Am. Chem. Soc.* **1992**, *114*, 7489−7493.

(13) Farnan, I.; Grandinetti, P. J.; Baltisberger, J. H.; Stebbins, J. F.; Werner, U.; Eastman, M. A.; Pines, A. *Nature* **1992**, *358*, 31−35.

(14) Smith, S.; Levante, T. O.; Meier, B. H.; Ernst, R. R. *J. Magn. Reson.* **1994**, *106*, 75−105.

(15) The programming environment GAMMA is available free of charge through the National High Magnetic Field Laboratory. Tallahassee, using the World Wide Web network (http://www.magnet.fsu.edu/~gamma/).

(16) Baldus, M.; Levante, T. O.; Meier, B. H. *Z. Naturforsch.* **1994**, *49a*, 80−88.

(17) Cheng, V. B.; Suzukawa, H. H.; Wolfsberg, M. J. *J. Chem. Phys.* **1973**, *59*, 3992−3999.

(18) MINUIT is part of the PACKLIB program package and was obtained under the conditions of the CERN Program Library/Division CN, CERN, CH-1211 Geneva, Switzerland.

(19) Bärlocher, C. *X-ray Rietveld System XRS-82*; Institut für Kristallographie und Petrographie, ETH Zürich, 1982.

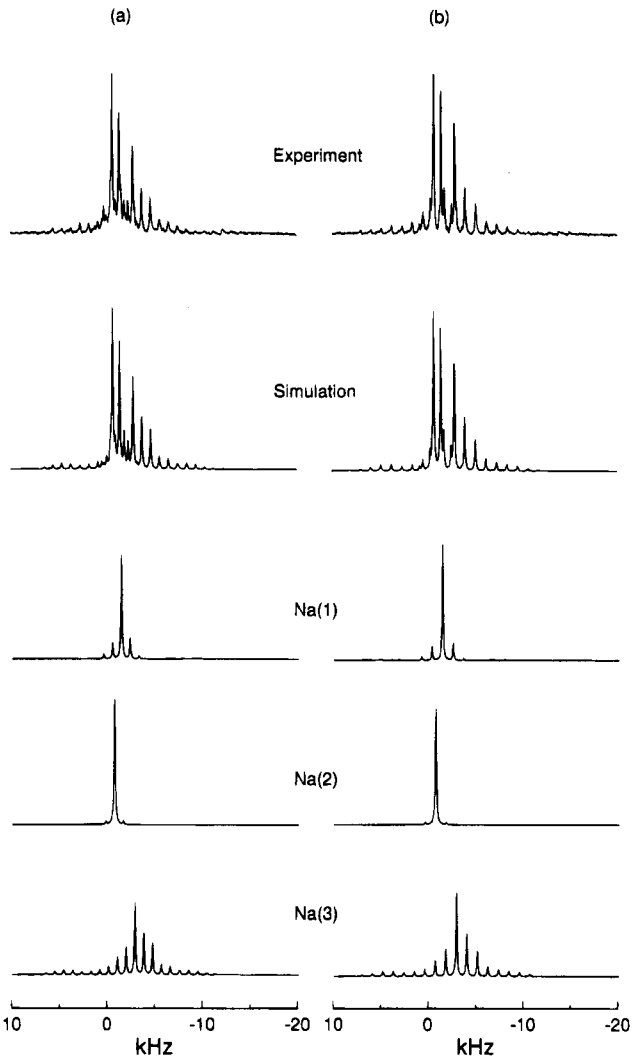

Figure 2. Nonsynchronized ^{23}Na DOR experiments at 11.7 T for two sets of [inner rotor, outer rotor]-spinning speeds together with the computer simulation described in the text: (a) [5470 Hz, 925 Hz]; (b) [5350 Hz, 1100 Hz]. In addition, the constituent parts of the spectrum resulting from the individual sodium sites are shown (numbering according to structure refinement; see Tables 1, 3, and 5).

shift can be replaced by its isotropic value. Due to the second inequality in eq 2, this simplified form can also be used in the presence of rotational sidebands because these are described, in good approximation, by the time dependence of the quadrupolar interaction only. The experimental spectra shall therefore be described by a one-spin model (in the rotating frame) Hamiltonian for each site i

$$H_i^{(ct)}(t) = \delta_i \omega_0 I_{iz} + \frac{\omega_{Q,i}^2}{2\omega_0} \sum_{m=-2}^{2} \frac{1}{m} G_m^{Lab,(i)}(t)[T_{2m}^{(i)}, T_{2,-m}^{(i)}] \quad (m \neq 0) \quad (5)$$

where δ_i denotes the isotropic chemical shift and ω_0 the Larmor frequency. For simplicity, we will omit in the following the site index i. The quadrupolar coupling constant ω_Q is related to the electric field gradient eq and the nuclear quadrupole moment Q by

$$\omega_Q = \frac{e^2 qQ}{2I(2I-1)\hbar} \quad (6)$$

The geometrical factors $G_m^{Lab}(t)$ depend on the instantaneous orientation of the principal axes system of the quadrupolar interaction in the laboratory frame of reference and on the quadrupole asymmetry parameter. They are discussed in detail in the Appendix. The irreducible spin tensor components T_{2m} are also given in the Appendix.

For MAS, the factors $G_m^{Lab}(t)$ take the form

$$G_m^{Lab}(t) = \sum_{m_1,m_2} G_m^{MAS}(m_1,m_2) \exp(-i\omega_R t(m_1 + m_2)) \quad (7)$$

and for DOR they are defined as

$$G_m^{Lab}(t) = \sum_{n_1,n_2,m_1,m_2} G_m^{DOR}(n_1,n_2,m_1,m_2) \exp(-i\omega_{R_1} t(n_1 + n_2)) \exp(-i\omega_{R_2} t(m_1 + m_2)) \quad (8)$$

where ω_R denotes the MAS angular frequency, and ω_{R_1} and ω_{R_2} are the inner and outer rotor angular frequencies in DOR. G_m^{MAS} and G_m^{DOR} are given in the Appendix. Insertion of eq 7 in eq 5 leads to a Fourier series expansion of the Hamiltonian $H^{(ct)}(t)$, and the equation of the motion can be solved using the Floquet formalism.[20-22] As an alternative approach, the time evolution can be broken up into short time intervals with a piecewise time-independent Hamiltonian. The Floquet approach is, however, more straightforward when applied in the framework of the simulation environment GAMMA.[14]

For DOR experiments, two basic frequencies ω_{R_1} and ω_{R_2} need to be considered and a two-mode Floquet approach can be taken.[16] A detailed discussion of this approach can be found in refs 22-24.

To determine the spectral parameters from Figure 1, a combination of grid and gradient search procedure using a least-squares fitting criterion was applied. For each of the three sodium sites, ω_Q and η were chosen and the free induction decay (fid) was simulated. The fit was restricted to the centerband of the $m_I = \pm 1/2$ transition, and a grid with a resolution of ± 1 kHz for the quadrupolar coupling and ± 0.01 for the asymmetry parameter η was used. As additional variables we introduced the isotropic chemical shifts δ and a Lorentzian line broadening (LB) for each of the three resonances. A variable dead time at the beginning of the calculated fid was introduced to account for phase distortions. The site population numbers were chosen according to crystal symmetry considerations. Finally, a variable parameter for the absolute intensity of the spectrum was taken into account. Thus, a total number of 14 variable parameters results.

In Figure 1, the least-squares-fitted simulation on the basis of three sodium resonances with intensity ratio 1:1:2 is given (solid line) and compared to the experimental data. In Table 1, we summarize the resulting parameters. The fitted dead time at the beginning of the fid is 9.2 ± 2 μs. The error intervals were obtained from a numerical multivariate error analysis.[25]

The quality of the fit in Figure 1 is measured by the normalized squared deviation $\epsilon^2 = \sum_{n=0}^{NP}[I_{SIM}(n) - I_{EXP}(n)]^2 / \sum_{n=0}^{NP} I_{EXP}^2(n)$. NP represents the number of sampling points (here NP = 872). For Figure 1 we find an excellent fit with $\epsilon^2 = 0.0064$.

(20) Shirley, J. H. *Phys. Rev. B* **1965**, *138*, 979-987.
(21) Vega, S.; Olejniczak, F. T.; Griffin, R. G. *J. Chem. Phys.* **1984**, *80*, 4832-4840.
(22) Levante, T. O.; Baldus, M.; Meier, B. H.; Ernst, R. R., manuscript in preparation.
(23) Ho, T. S.; Chu, S. I.; Tietz, J. V. *Chem. Phys. Lett.* **1983**, *99*, 422-426.
(24) Chu, S. *Adv. Chem. Phys.* **1989**, *73*, 739-799.
(25) Clifford, A. A. *Multivariate Error Analysis*; Applied Science Publishers Ltd.: Essex, 1973.

Table 1. Sodium-23 NMR Fit Parameters Obtained from a Combined Grid and Gradient Search Procedure Using a Least-Squares Fitting Criterion[a]

site	rel pop	ω_Q (kHz)	η	δ (ppm)[b]	LB (Hz)[c]
Na(1)	1	355 ± 12	0.69 ± 0.05	5.52 ± 0.20	29.3 ± 3.2
Na(2)	1	229 ± 7	0.21 ± 0.03	6.20 ± 0.15	31.4 ± 1.1
Na(3)	2	617 ± 8	0.27 ± 0.02	7.24 ± 0.12	33.8 ± 5.0

[a] For the error analysis, the error of a single measurement point was estimated to 1% of the highest intensity in the spectrum. [b] The isotropic shift values δ are given relative to 0.1 M NaCl. [c] Full width at half-height (fwhh).

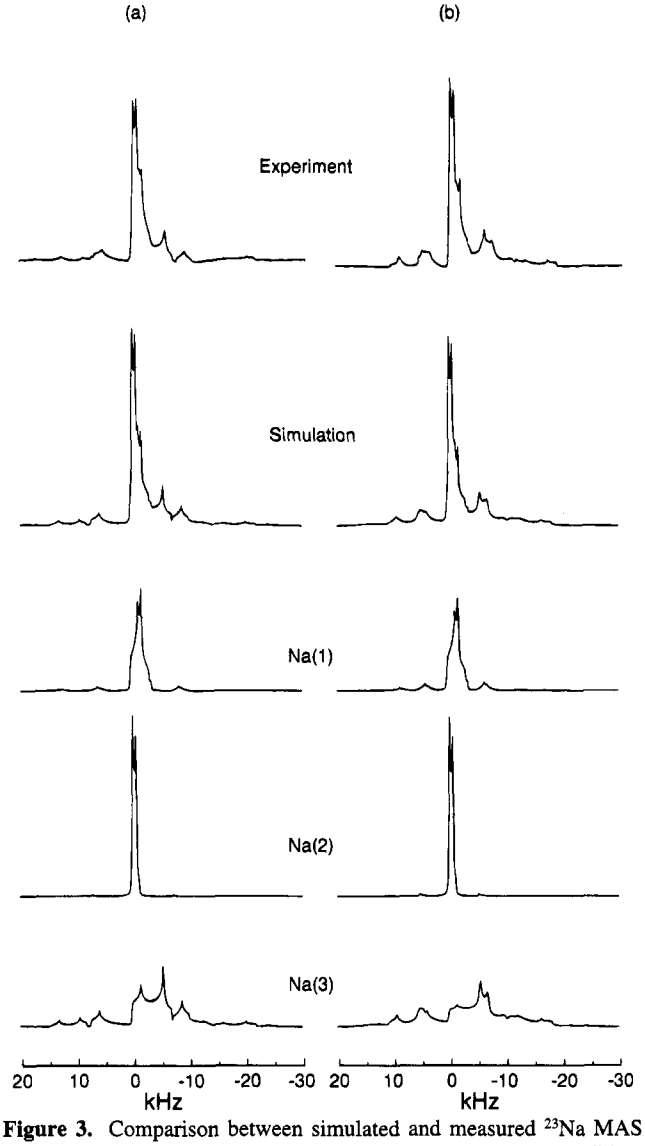

Figure 3. Comparison between simulated and measured ^{23}Na MAS spectra at 7 T for (a) 7200 and (b) 5230 Hz spinning speed. In addition, the individual contributions of the three sodium sites are shown.

The parameter values of Table 1 were then used to predict spectra in a lower magnetic field of 7 T and for different spinning speeds. Here, contributions from the MAS sidebands of the three sites as well as line shape changes of the centerbands lead to a complicated overlapping composite as shown in Figure 3. Computed MAS spectra are shown for spinning speeds of 7200 and 5230 Hz. The sideband pattern at lower fields is dominated by the Na(3) quadrupole tensor. A comparison between recorded and calculated spectra (Figure 3) shows that parameters retrieved from the experiment of Figure 1 result in consistent spectra at a field of 7 T.

Finally, the parameters of Table 1 were used to simulate the nonsynchronized DOR spectra for the experimental conditions of Figure 2. Perfect agreement is obtained. Similar to the MAS experiments in lower field, the sideband pattern is dominated by the relatively large quadrupole tensor of the Na(3) site. In summary, all NMR data can be consistently explained using the spectral parameters of Table 1.

(b) Structure Determination. To reconcile the NMR results with the X-ray data, the structure of anhydrous disodium hydrogen phosphate was reinvestigated by a Rietveld refinement of powder XRD data. This approach was necessary because of the problems in obtaining single crystals of sufficient size and quality. With the published structure, a good starting model for the refinement was available.

A careful investigation of the powder XRD data revealed some weak reflections (see arrows in Figure 4) that cannot be indexed on the basis of the previously reported structure[1] but require a doubling of the unit cell as proposed in ref 3. We checked possible space groups and unit cells that are feasible according to group−subgroup relations.[26,27] The space group $P2_1/c$ gave the best agreement with the observed superstructure reflections. It strictly meets all reflection conditions and can explain the 1:1:2 population of the sites observed by ^{23}Na NMR. Thus, the HPO_4 group is no longer constrained to exhibit mirror symmetry, and an ordered arrangement of the protons is feasible.

To refine the structure in space group $P2_1/c$, the collected powder XRD data were background-corrected and a standard peak shape function was calculated using the (102) reflection at $2\theta = 31.03°$. The positional parameters of model A were transformed into the space group $P2_1/c$, and the isotropic averages of the thermal parameters were estimated. These data were used as starting values for the refinement.

First, peak half-widths and asymmetries and their angular dependence were refined over the whole profile. The unit cell parameters were optimized followed by an empirical correction of the 2θ scale. Before refining any positional parameters, geometrical constraints were applied to the phosphate group in order to keep bond lengths and angles within reasonable limits. As the refinement progressed, the weights of these constraints were lowered and finally released. Atomic positions and individual isotropic temperature factors were optimized alternatingly until the refinement converged with an R_{wp} value of 0.086 (for definition of R_{wp}, see Table 2).

Strong correlations were found for the thermal parameters of atoms Na(1) and Na(2) as well as for the thermal and positional parameters of atoms O(3) and O(4). Thus, the correlated thermal parameters were constrained to be equal. These correlations can be understood in terms of an approximate pseudosymmetry where the deviation from mirror symmetry is rather small. Nevertheless, it is significant, as we will show later.

Attempts to locate the proton by calculation of the residual electron density failed. The difference electron density did not show features that could be associated with hydrogen positions. However, since atom O(4) shows the longest P−O bond, we concluded that it should be carrying the proton. Furthermore, it exhibited the shortest interatomic distance of 250 pm to oxygen O(3) of a neighboring PO_4 tetrahedron. Thus we searched for a proton position between O(4) and O(3) that fulfilled the following conditions: (i) The bond distance O(4)−H should be about 107 pm. This is the value found by neutron-diffraction studies of hydrogen-bonded inorganic salts. (ii) The angle P−O(4)−H should be about 104.5°, which is the angle of the free water molecule. (iii) The distances to all four neighboring Na atoms should be maximum.

(26) Hahn, Th., Ed. *International Tables for Crystallography*. Kluwer Academic Publishers: Dordrecht, 1992; Vol. A.
(27) Bärnighausen, H. *MATCH, Commun. Math. Chem.* **1980**, *9*, 139−175.

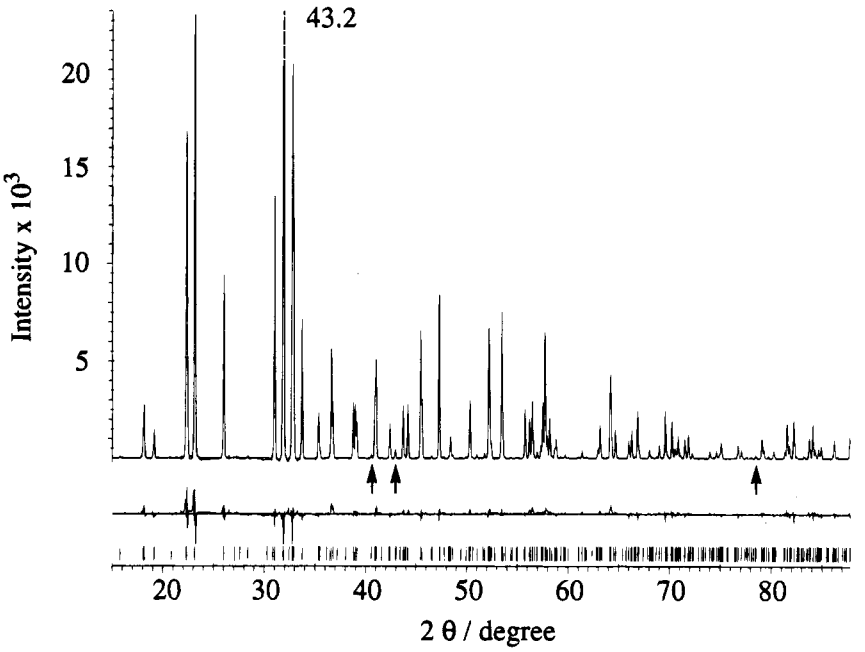

Figure 4. Observed and calculated powder X-ray diffraction intensities (top) and their difference (bottom) for Na_2HPO_4. The peak of highest intensity (I = 43200 arb units) is cut off to show sufficient details. Vertical bars mark the positions of symmetry-allowed reflections. Arrows indicate the superstructure reflections with highest intensities.

Table 2. Crystallographic Data on the Rietveld Refinement of Na_2HPO_4

Unit Cell	
space group	$P2_1/c$
a (Å)	5.450(2)
b (Å)	6.845(1)
c (Å)	10.944(3)
β (deg)	116.35(9)
unit cell vol (Å^3)	365.8(3)
Z	4
Refinement	
standard peak (102)	$2\theta = 31.03°$
peak range (in units of fwhm)	10.0
no. of observations (N)	3369
no. of contributing reflections	273
no. of geometric restraints	10
no. of structural parameters ($P1$)	28
no. of profile parameters ($P2$)	12
R_{exp}[a]	0.066
R_{wp}[b]	0.084
R_F[c]	0.074

[a] $R_{exp} = [(N - P1 - P2)/\sum wy^2(\text{obs})]^{1/2}$ (statistically expected R value). [b] $R_{wp} = \{\sum w[y(\text{obs}) - y(\text{calc})]^2/\sum wy^2(\text{obs})\}^{1/2}$ (weighted profile R value). [c] $R_F = \sum|F(\text{obs}) - F(\text{calc})|/\sum F(\text{obs})$ (R value of structure factors).

Optimization of these distances and angles was done by a least-squares procedure.[19] After inclusion of the optimized proton position into the refinement and careful adjustment of its temperature factor, the R_{wp} value dropped (insignificantly) to 0.084. The final agreement between the observed and calculated profiles is satisfactory as can be seen in Figure 4. Crystallographic refinement data are collected in Table 2. The atomic positions and temperature factors of model B are given in Table 3, and a plot of the unit cell is shown in Figure 5. Table 4 gives some relevant distances and angles.

To evaluate the significance of the difference between models A and B, we calculated the R_{wp} value of model A for our data by keeping the general profile variables obtained from the refinement of model B fixed, using the positional parameters of model A and refining the isotropic temperature factors only. R_{wp}(A) was found to be 0.105 (R_F(A) = 0.084) while R_{wp}(B) is 0.084 (R_F(B) = 0.074). Thus we conclude that the differences in atomic positions are indeed significant. The strongest evidence from the X-ray experiments, however, is the fact that only on the basis of a doubled unit cell with space group $P2_1/c$ can all observed reflections be indexed properly and obey the extinction rules.

Table 3. Positional and Isotropic Thermal Parameters for Na_2HPO_4 (Model B)[a]

atom	x	y	z	U (pm^2)
Na(1)	0	0	0	163(6)
Na(2)	0	0.5	0	163(6)[b]
Na(3)	0.3921(3)	0.2355(9)	0.3883(2)	249(7)
P	0.6658(3)	0.2513(9)	0.1909(2)	125(4)
O(1)	0.3574(5)	0.2465(16)	0.1060(2)	92(10)
O(2)	0.7643(5)	0.2521(14)	0.3436(3)	66(10)
O(3)	0.7968(17)	0.4229(9)	0.1465(7)	65(9)
O(4)	0.7858(17)	0.4464(10)	0.6567(8)	65(9)[c]
H	0.0322[d]	0.5199[d]	0.2529[d]	482[d]

[a] Numbers in parentheses are estimated standard deviations (esd's) in units of the least significant digit given. [b] Constrained to be equal to U of Na(1). [c] Constrained to be equal to U of O(3). [d] Esd's are not given since the parameters of the proton were not refined.

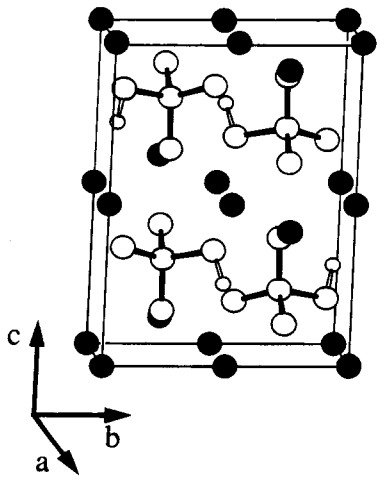

Figure 5. Unit cell of the structure of Na_2HPO_4 (model B): filled circles, Na atoms; small open circles, H atoms; large open circles, P and O atoms.

Table 4. Selected Interatomic Distances (pm) and Angles (deg)

distances		angles	
Na(1)−O(1)	245 (2×)	O(1)−Na(1)−O(2)	84.8
Na(1)−O(2)	235 (2×)	O(1)−Na(1)−O(4)	84.8
Na(1)−O(4)	249 (2×)	O(2)−Na(1)−O(4)	82.9
Na(1)−H	279 (2×)	O(1)−Na(2)−O(2)	83.7
Na(2)−O(1)	248 (2×)	O(1)−Na(2)−O(3)	88.1
Na(2)−O(2)	237 (2×)	O(2)−Na(2)−O(3)	86.6
Na(2)−O(3)	238 (2×)	O(1)−Na(3)−O(2)	131.0
Na(2)−H	270 (2×)	O(1)−Na(3)−O(3)	89.2
Na(3)−O(1)	248	O(1)−Na(3)−O(4)	87.4
Na(3)−O(2)	229	O(2)−Na(3)−O(3)	112.3
Na(3)−O(3)	233	O(2)−Na(3)−O(4)	103.4
Na(3)−O(4)	234	O(3)−Na(3)−O(4)	135.0
Na(3)−H	260	O(1)−P−O(2)	115.5
Na(3)−H	269	O(1)−P−O(3)	111.2
P−O(1)	152	O(1)−P−O(4)	107.0
P−O(2)	151	O(2)−P−O(3)	110.8
P−O(3)	156	O(2)−P−O(4)	106.1
P−O(4)	162	O(3)−P−O(4)	105.7
P−H	217	P−O(3)−H	117.2
O(1)−O(2)	256	P−O(4)−H	105.7
O(1)−O(3)	254	O(3)−H−O(4)	164.8
O(1)−O(4)	252		
O(2)−O(3)	253		
O(2)−O(4)	250		
O(2)−H	243		
O(3)−O(4)	253		
O(3)−O(4)	250		
O(3)−H	145		
O(4)−H	107		

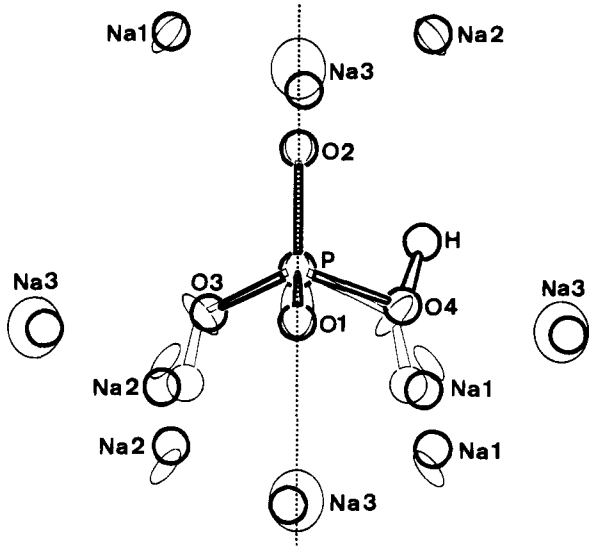

Figure 6. Plot of the local environment of the HPO_4^{2-} anions in models A (ellipsoids, thin lines) and B (circles, thick lines), respectively. Note the loss of the mirror plane due to the lower symmetry of model B. The ellipsoids of model A are shown for 70% probability.[1] The atoms of model B, shown as circles of uniform size, are labeled according to Table 3.

In Figure 6 we display the geometry of models A and B including the thermal ellipsoids published for model A (ORTEP plot,[28] thermal displacement for 70% probability). There is a good correlation between the ellipsoids in the high-symmetry model A with the positional shifts found for model B. We take this as another support for structure B.

The structure of anhydrous Na_2HPO_4 can be described by hydrogen-bonded zigzag chains of phosphate anions in the direction of the *b*-axis (Figure 7). The relative orientation of

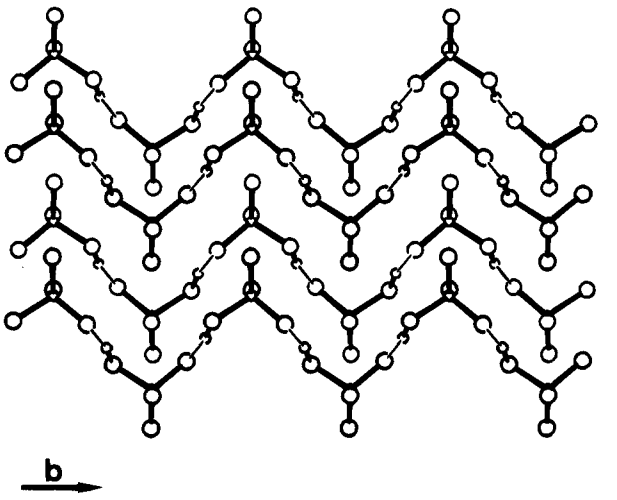

Figure 7. View of the structure of anhydrous Na_2HPO_4 along direction [101]. The hydrogen-bonded HPO_4^{2-} anions form parallel zigzag chains in the directions of the *b* axis. Na atoms are left out for clarity.

the phosphate anions and the resulting hydrogen-bonded chains is a direct consequence of the space group. The short distance between O(3) and O(4) is typical for a strong hydrogen bond. As can be seen from Table 4, atoms Na(1) and Na(2) have a slightly distorted octahedral coordination by six oxygens. In contrast, Na(3) has a strongly distorted tetrahedral surrounding of oxygen atoms and shows the shortest distances to protons. The P−O bond distances and the bond angles at the phosphorus are close to values reported in the literature.[3] Only the relatively long P−O(3) bond is out of the normal range. This might be easily explained by the strong hydrogen bonding in which only O(3) takes part but not O(1) and O(2).

(c) Assignment of the ^{23}Na NMR Resonances to the Crystallographic Sites. The entire analysis performed so far does not require an assignment of the ^{23}Na resonance lines. For completeness, we now proceed to assign the ^{23}Na NMR resonances to the three sites of the structure. The number of sodium atoms per unit cell is 2, 2, and 4 for Na(1), Na(2), and Na(3), respectively. Because of its intensity, the line with the largest quadrupole coupling can be unambiguously assigned to site Na(3). The Na(1) and Na(2) resonances result from the distorted octahedral sites.

Koller et al.[29] have found that the quadrupolar coupling constant of ^{23}Na compounds can be estimated using a simple model where only the oxygen nuclei of the first coordination sphere are taken into account as effective point charges. The effective charges of each of the four oxygen sites were determined, using model 1 of ref 29, as $q_i = (-2 + \sum_j f_{ij})e$, where -2 is the formal charge of each oxygen and f_{ij} is the covalence of the oxygen (i)−cation (j) bond. The f_{ij} have been calculated by the empirical equations of Brown and Shannon,[30] taking into account the directly coordinating phosphorus, sodium, and hydrogen atoms. As effective oxygen charges, we find $q_1 = -1.02$ e, $q_2 = -1.01$ e, $q_3 = -1.02$ e, and $q_4 = -1.04$ e.

Using these values and the crystal structure determined in this work, the electrical field gradients and hence the quadrupolar coupling constants at the three sodium sites can be determined. Assuming a quadrupole moment[31] $Q = 0.102 \times 10^{-28}$ m^2 and

(28) Johnson, C. K. *ORTEP II, Thermal Ellipsoid Plot Program*, Oak Ridge, TN, 1976.

(29) Koller, H.; Engelhardt, G.; Kentgens, A.P.M.; Sauer, J. *J. Phys. Chem.* **1994**, *98*, 1544−1551.

(30) Brown, I. D.; Shannon, R. D. *Acta Crystallogr., Sect. A* **1973**, *29*, 266−282.

(31) Lederer, M.; Shirley, V. S. *Table of Isotopes*, 7th ed.; Wiley-Interscience: New York, 1978.

Table 5. Comparison between the Quadrupolar Coupling Constants Obtained from Numerical Simulations of NMR Experiments (exp; See Table 1) and Calculated Values (cal)[a]

site	N^b	I^c	$\omega_{Q,exp}$ (kHz)	$\omega_{Q,cal}$ (kHz)
Na(1)	2	1	355 ± 12	331
Na(2)	2	1	229 ± 7	217
Na(3)	4	2	617 ± 8	634

[a] The calculations were performed on the basis of the XRD results using a simple point charge model. [b] Number of atoms per unit cell. [c] Relative intensity of ^{23}Na NMR signals.

a Sternheimer antishielding factor[32] of 4.56 for ^{23}Na and using the computer program of ref 29, we obtain the quadrupolar coupling constants of Table 5. The asymmetry parameters are not given as they are known to be ill-determined by this simple approach. The correspondence between experimental quadrupolar coupling constants and calculated ones is astonishingly good, and we therefore assign the larger quadrupole splitting to Na(1).

Conclusions

Based on the NMR and X-ray measurements reported in this article, anhydrous Na_2HPO_4 crystallizes in a monoclinic $P2_1/c$ structure rather than the previously reported $P2_1/m$ space group. The analysis of the experimental rotating and double-rotating NMR data was facilitated by an extended Floquet approach. The recorded spectra can be analyzed even in the case of severe overlap of several resonances, and the comparison between MAS and DOR results offers a direct way for testing the consistency of the retrieved parameters.

Renewed powder XRD measurements and a subsequent structure refinement on the basis of the new space group led to new atomic positions. Due to its double intensity, the NMR signal with the largest quadrupolar coupling could be assigned easily to the crystallographic site Na(3). Using the new crystal structure data, the quadrupolar coupling constants for all three inequivalent sodium sites were estimated using a simple point charge model. Good agreement between measured and calculated quadrupolar coupling constants was achieved, and the remaining two resonances were assigned to crystallographic sites Na(1) and Na(2), respectively.

The combination of NMR, numerical simulation, and X-ray diffraction techniques offers a powerful tool for structural investigations. In the present example, the strong dependence of the quadrupolar interaction on the relatively minor differences in atomic coordinates leads to a clear distinction between possible space groups while the diffraction pattern depends only weakly on these differences. Once the reported space group was shown to be incorrect by NMR, the determination of the correct space group based on the X-ray and NMR data led to an improved structure refinement. Thus, the structural information retrieved from the complementary methods can overcome problems which may not be solved by one method alone.

Acknowledgment. We thank Dr. S. Steuernagel for measuring high-field MAS and DOR spectra at Bruker Analytische Messtechnik, Rheinstetten/Germany. This work was supported by the Schweizerischer Nationalfonds. M.B. gratefully acknowledges financial support by the Stipendienfonds der Basler Chemischen Industrie.

Appendix

The irreducible tensor components T_{2m} for the quadrupolar interaction can be defined in terms of the spherical angular momentum operators (I_z, $I^{\pm}$) as

$$T_{20} = \frac{1}{\sqrt{6}}(3I_z^2 - I^2), \qquad T_{2,\pm1} = \frac{\mp 1}{2}(I_z I^{\pm} + I^{\pm} I_z),$$

$$T_{2,\pm2} = \frac{1}{2}(I^{\pm})^2 \quad \text{(A.1)}$$

The geometrical factor $G_m^{Lab}(t)$ in eq 4 can be identified with the product

$$G_m^{Lab}(t) = A_{2m}^{Lab} A_{2,-m}^{Lab} \quad \text{(A.2)}$$

To calculate the elements of the second rank irreducible spatial tensor A_{2m}^{Lab} in the laboratory (Lab) frame for MAS, we first perform an Euler transformation (defined by the angles φ,θ,χ) from the rotor-fixed axes system (RAS) to the principal axes system of the quadrupole tensor. The elements of the spatial tensors in the rotor-fixed axes system can be written as

$$A_{20}^{RAS} = \left(\frac{3}{8}\right)^{1/2}[(3\cos^2\theta - 1) + \eta \sin^2\theta \cos 2\chi]$$

$$A_{2,\pm1}^{RAS} = -\frac{1}{2}\sin\theta\, e^{\pm i\varphi}[\pm(3 - \eta\cos 2\chi)\cos\theta + i\eta \sin 2\chi]$$

$$A_{2,\pm2}^{RAS} = \frac{1}{2}e^{\pm i2\varphi}\left[\frac{3}{2}\sin^2\theta + \frac{\eta}{2}(1 + \cos^2\theta)\cos 2\chi \mp i\eta\cos\theta \sin 2\chi\right] \quad \text{(A.3)}$$

where the asymmetry parameter of the quadrupolar coupling tensor is denoted by η.

Using the components of the Wigner rotation matrices $d^{(2)}_{m'm}(\Theta_1)$ that relate the RAS to the Lab frame, we find

$$G_m^{Lab}(t) = A_{2m}^{Lab} A_{2,-m}^{Lab} = \sum_{m_1,m_2} A_{2m_1}^{RAS} A_{2,-m_2}^{RAS} d^{(2)}_{m_1 m}(\Theta_1) d^{(2)}_{m_2,-m}(\Theta_1) \exp(-i\omega_R t(m_1 + m_2)) \quad \text{(A.4)}$$

with $\Theta_1 = 54.74°$. With the abbreviation

$$G_m^{MAS}(m_1,m_2) = A_{2m_1}^{RAS} A_{2,-m_2}^{RAS} d^{(2)}_{m_1 m}(\Theta_1) d^{(2)}_{m_2,-m}(\Theta_1)$$

eq 7 is obtained.

An analogous treatment of a DOR experiment requires two independent time-dependent transformations from the inner rotor axes system (IRAS) to the laboratory frame:

$$G_m^{Lab}(t) = A_{2m}^{Lab} A_{2,-m}^{Lab} = \sum_{n_1,n_2,m_1,m_2} A_{2n_1}^{IRAS} A_{2n_2}^{IRAS} d^{(2)}_{n_1 m_1}(\Theta_2) d^{(2)}_{n_2 m_2}(\Theta_2) d^{(2)}_{m_1 m}(\Theta_1) d^{(2)}_{m_2,-m}(\Theta_1) \exp(-it((n_1 + n_2)\omega_{R_1} + (m_1 + m_2)\omega_{R_2})) \quad \text{(A.5)}$$

Here, Θ_1 and Θ_2 denote the rotor axes angles that are given by $\Theta_1 = 54.74°$ and $\Theta_2 = 30.56°$, respectively. With the definition

$$G_m^{DOR}(n_1,n_2,m_1,m_2) = A_{2n_1}^{IRAS} A_{2n_2}^{IRAS} d^{(2)}_{n_1 m_1}(\Theta_2) d^{(2)}_{n_2 m_2}(\Theta_2) d^{(2)}_{m_1 m}(\Theta_1) d^{(2)}_{m_2,-m}(\Theta_1) \quad \text{(A.6)}$$

eq 8 is obtained.

(32) Sternheimer, R. M. *Phys. Rev.* **1959**, *115*, 1198−1206.

JA943876C